JACS
JOURNAL OF THE AMERICAN CHEMICAL SOCIETY

Article

pubs.acs.org/JACS

Steering Metallofullerene Electron Spin in Porous Metal–Organic Framework

Yongqiang Feng, Taishan Wang,* Yongjian Li, Jie Li, Jingyi Wu, Bo Wu, Li Jiang, and Chunru Wang*

Beijing National Laboratory for Molecular Sciences, Key Laboratory of Molecular Nanostructure and Nanotechnology, Institute of Chemistry, Chinese Academy of Sciences, Beijing 100190, China

Supporting Information

ABSTRACT: Paramagnetic endohedral fullerenes are ideal candidates for quantum information processing and high-density data storage due to their protected spins with particularly high stability. Herein, we report a solid spin system based on a paramagnetic metallofullerene $Y_2@C_{79}N$ through incarcerating it into the cage-shaped pores of a metal–organic framework (MOF-177). In this kind of guest and host complex, the $Y_2@C_{79}N$ molecules inside the pores of MOF crystal show axisymmetric paramagnetic property. It was found that the pores of MOF-177 crystal play an important role in dispersing the $Y_2@C_{79}N$ molecules as well as in steering their electron spin. The group of arranged $Y_2@C_{79}N$ molecules and their electron spins in MOF crystals are potential quantum bits for quantum information science and data storage. Moreover, this kind of solid spin system can be used as a probe for nanoscale nuclear magnetic resonance or for motion imaging of a single biomolecule.

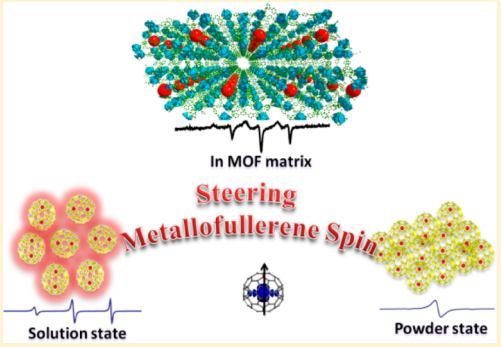

INTRODUCTION

Manipulation of the electron spin has attracted widespread interests of scientists from physics, chemistry, and material sciences,[1] taking into account its growing potential advantages in quantum information processing and data storage.[2] Of spectacular importance in spin-carrier is endohedral fullerenes,[3] among which $N@C_{60}$, $Sc_3C_2@C_{80}$ and $Y_2@C_{79}N$, etc., have been expected to be excellent candidates as qubits for quantum computers due to their unique magnetic properties and favorable coherence time.[4] Notably, the arrangement of these spin-active endohedral fullerenes in solid state is essential for further quantum computing.[5] An attempt is to group them together inside carbon nanotubes (CNTs) to form peapod structure.[6] Recently, the metal–organic frameworks (MOFs) have been intriguing many interests due to their porous structures and excellent crystallinity.[7] Particularly, the ordered nanosized pores in MOF crystals make them good host for these endohedral fullerenes.[8]

$Y_2@C_{79}N$ is a very important spin-active endohedral fullerene, in which the nitrogen atom substitutes for one of the C_{80} carbon atoms and introduces one unpaired electron spin.[9] The electronic structure of $Y_2@C_{79}N$ resembles the single negatively charged nitrogen-vacancy (NV^-) color centers in diamond,[10] which are considered to be solid state spin qubit suitable for quantum information processing and quantum metrology devices. Moreover, the $Y_2@C_{79}N$ offers a possibility to construct spin system in solid state via a bottom-up approach. In previous report of fullerene-containing host–guest complex, the fullerene carbon cages are always prone to interact with the planar aromatic motif of the host molecules through strong $\pi-\pi$ interactions.[8,9a] In MOF structures, there are many similar planar aromatic contents.[7] For example, MOF-177,[7e] formulated as $Zn_4O(BTB)_2$ (BTB = 4,4′,4″-benzene-1,3,5-triyltribenzoate), its cage-shaped pore has two sets of parallel quasi-planar triphenylbenzene unit, 14 Å apart from each other. Therefore, the MOF-177 can well accommodate $Y_2@C_{79}N$ and the ordered pores of MOF would induce the directional arrangement of $Y_2@C_{79}N$, leading to special solid state spin system.

Herein, we report the preparation and paramagnetic property of spin-active endohedral fullerene $Y_2@C_{79}N$ accommodating in MOF-177 crystals through a bottom-up approach. Interestingly, in $Y_2@C_{79}N\subset$MOF-177 complex, the $Y_2@C_{79}N$ molecules tend to reside along the *c*-axis of MOF-177 crystal lattice under low temperature as disclosed by its axisymmetric electron spin resonance (ESR) characters. The confined effect of MOF's pores plays a significant role in steering the electron spin on endohedral fullerene, leading to anisotropic paramagnetic solid system that is applicable for high-density data storage. Moreover, the paramagnetic $Y_2@C_{79}N\subset$MOF-177 single crystal can be used as a probe for nanoscale nuclear magnetic resonance detection.

RESULTS AND DISCUSSION

Preparation and Characterizations of $Y_2@C_{79}N\subset$MOF-177 Complex. $Y_2@C_{79}N$ has a nitrogen atom substituting for one of the C_{80} carbon atoms and its diameter is about 8 Å,[9] as

Received: October 15, 2015
Published: November 13, 2015

DOI: 10.1021/jacs.5b10796
J. Am. Chem. Soc. 2015, 137, 15055–15060

shown in Figure 1a. $Y_2@C_{79}N$ is an open-shell molecule and there is an unpaired electron locating on the internal Y_2 cluster,

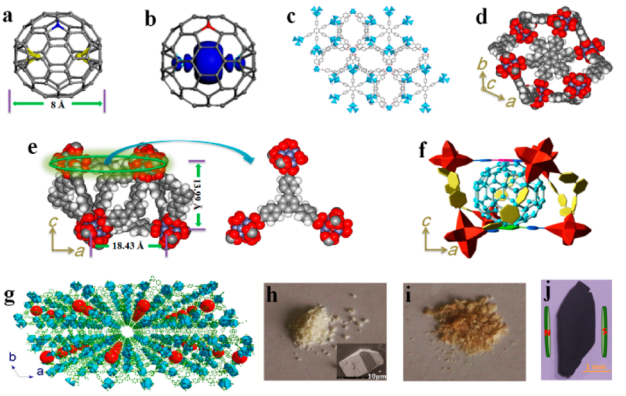

Figure 1. (a) Optimized structure of $Y_2@C_{79}N$. (b) Calculated spin density distributions of $Y_2@C_{79}N$. (c) Crystallographic structure of MOF-177. Blue, Zn; red, O; gray, C. H atoms and guest molecules are omitted for clarity. Cage-shaped pore of MOF-177 along *c* axis (top view, d) and along *b* axis (side view, e). (f) Schematic drawing of the inclusion of $Y_2@C_{79}N$ inside the cavity of MOF-177. The orientation of $Y_2@C_{79}N$ standing inside the pores of MOF-177 is in the manner that the N atom (dark blue) on the carbon cage is adjacent to the triphenylbenzene unit. (g) Schematic drawing of $Y_2@C_{79}N\subset$MOF-177 complex. Color code: blue, Zn; yellow, O; green, C; red, $Y_2@C_{79}N$. H atoms and guest molecules are omitted for clarity. (h) Optical image (inset: an SEM image of a crystal) of synthesized MOF-177 crystals. The crystal is in the shape of polyhedral block in micron scale. (i) Optical image of $Y_2@C_{79}N\subset$MOF-177 complex. (j) A selected single crystal of $Y_2@C_{79}N\subset$MOF-177 for varied temperature ESR measurements.

as shown in Figure 1b. The crystal of MOF-177 was synthesized by heating zinc nitrate with H_3BTB.[7e] This trigonal porous framework has numerous cage-shaped pores, as shown in Figure 1c. Its cage-shaped pore has two sets of parallel quasi-planar triphenylbenzene unit, whose distance is about 13.99 Å, as shown in Figure 1d and e. Furthermore, in the single crystal of $Tb_2@C_{79}N\cdot Ni(OEP)\cdot 2C_6H_6$ (OEP is the octaethylporphyrin), the distance of two Ni(OEP) units, trapped a $Tb_2@C_{79}N$, is about 14 Å.[9a] Therefore, the cage-shaped pore of MOF-177 can well accommodate one $Y_2@C_{79}N$ molecule through $\pi-\pi$ interactions, as shown in Figure 1f. Experimentally, 5 mg of MOF-177 crystals were immersed into toluene solution of $Y_2@C_{79}N$ for several days to let the $Y_2@C_{79}N$ enter the pores of MOF-177 completely. After removing the supernatant, the obtained complex (denoted as $Y_2@C_{79}N\subset$MOF-177) with orange color were washed with toluene for times and dried by nitrogen gas flow, as shown in Figure 1i.

To verify the encapsulation of $Y_2@C_{79}N$ into the nanosized channels of MOF-177, transmission electron microscopy (TEM), energy dispersive spectrometer (EDS), physisorption analysis, X-ray photoelectron spectrum (XPS), powder X-ray diffraction (PXRD) and inductively coupled plasma (ICP) analyses were performed (Figure 2, S4–S6). It can be seen clearly from Figure 2a–d that yttrium was well-distributed as carbon and zinc elements in $Y_2@C_{79}N\subset$MOF-177 crystal. EDS analysis (Figure 2e) and XPS measurement (Figure S5) for $Y_2@C_{79}N\subset$MOF-177 confirmed the existence of yttrium element originating from $Y_2@C_{79}N$. Furthermore, BET surface area shows a decrease from 894 $m^2\ g^{-1}$ in MOF-177 crystal to 721 $m^2\ g^{-1}$ in $Y_2@C_{79}N\subset$MOF-177 complex, indicating that

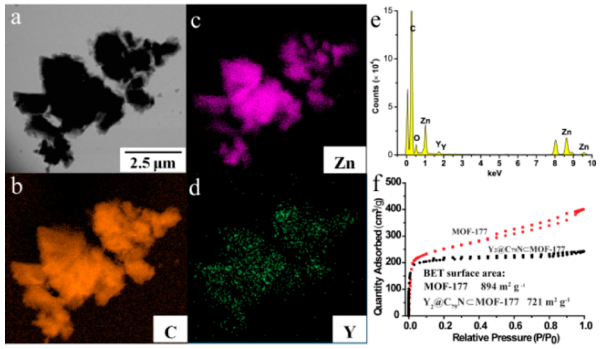

Figure 2. (a) TEM image of selected $Y_2@C_{79}N\subset$MOF-177 complex. TEM element mapping of C (b), Zn (c) and Y (d) for $Y_2@C_{79}N\subset$MOF-177 complex. (e) EDS file of $Y_2@C_{79}N\subset$MOF-177. (f) N_2 adsorption (circle) and desorption (square) isotherm curves of MOF-177 (red) and $Y_2@C_{79}N\subset$MOF-177 (black).

the $Y_2@C_{79}N$ molecules are encapsulated into the pore of MOF-177 rather than adsorbed on the crystal surface.[11] Moreover, PXRD spectrum (Figure S6) of the $Y_2@C_{79}N\subset$MOF-177 is obviously different from that of pristine MOF-177. The change appears at 2-theta value of around 6° corresponding to *d* value of about 15 Å, which is ascribed to the crystal lattice perturbation caused by $Y_2@C_{79}N$ incarceration.[7e] ICP result disclosed a weight ratio of 5.74% for $Y_2@C_{79}N$ in $Y_2@C_{79}N\subset$MOF-177.

Anisotropic ESR Analysis of $Y_2@C_{79}N\subset$MOF-177 Single Crystal. The paramagnetic properties of $Y_2@C_{79}N\subset$MOF-177 single crystal (Figure 1j) were carried out by means of continuous-wave ESR technique with X-band. It can be seen that at 293 K the $Y_2@C_{79}N\subset$MOF-177 presents a similar ESR spectrum with that of pristine $Y_2@C_{79}N$ in CS_2 solution (see Figure 3a,b), indicative of dispersive $Y_2@C_{79}N$ molecules within MOF-177. However, the line width of 10 G

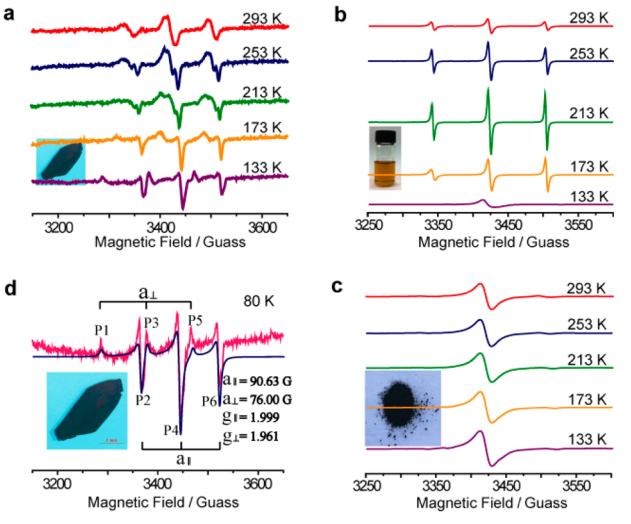

Figure 3. Temperature-dependent ESR spectra of $Y_2@C_{79}N\subset$MOF-177 single crystal (a), $Y_2@C_{79}N$ in CS_2 solution (b) and $Y_2@C_{79}N$ powders (c) at temperatures of 293, 253, 213, 173, and 133 K. (d) ESR spectrum of $Y_2@C_{79}N\subset$MOF-177 single crystal measured at 80 K. The simulated line (blue) is in good agreement with the experimental spectrum (pink), where P1, P3 and P5 correspond to the spin tensor along orthogonal orientation and P2, P4 and P6 belong to spin tensor at parallel direction.

DOI: 10.1021/jacs.5b10796
J. Am. Chem. Soc. 2015, 137, 15055–15060

for $Y_2@C_{79}N$⊂MOF-177 is nearly two times larger than that of pristine $Y_2@C_{79}N$ in CS_2 solution, which reveals that the $Y_2@C_{79}N$ in $Y_2@C_{79}N$⊂MOF-177 has increased spin−lattice interactions ascribed to the solid state spin system. Furthermore, when the temperature dropped to 253 K, the $Y_2@C_{79}N$⊂MOF-177 showed obvious anisotropic ESR peaks, i.e., the intensity of ESR line at high field specifically increased. This kind of anisotropy of $Y_2@C_{79}N$ can be ascribed to the changed interaction between spin angular momenta and the orbital angular momenta under low temperature,[9b] implying the insufficient rotational averaging in resonance structure.[12] For comparison, the temperature-dependent ESR measurements were executed on CS_2 solution of $Y_2@C_{79}N$ from 293 to 133 K. At 213 K, the ESR signals of $Y_2@C_{79}N$ in solution state also exhibit paramagnetic anisotropy, which is ascribed to the insufficient rotational averaging in resonance structure.

Unprecedentedly, for $Y_2@C_{79}N$⊂MOF-177, it was revealed that at or below 213 K the ESR spectra exhibit axisymmetric hyperfine splitting with hfcc values ($g_\perp$ and $g_\parallel$; $a_\perp$ and $a_\parallel$), indicating the $Y_2@C_{79}N$ molecules inside the pores of MOF-177 turn to an orientational state. And the 213 K can be considered as the "orientational transition"[13] point for the jailed $Y_2@C_{79}N$ within MOF-177 matrix. The experimental and simulated ESR spectra at 80 K were particularly shown in Figure 3d, in which the simulated spectrum is in good agreement with the experimental one with parameters of $a_\perp$ = 76.00 G, $a_\parallel$ = 90.63 G, $g_\perp$ = 1.961, and $g_\parallel$ = 1.999.

Generally, the anisotropic hyperfine interaction energy in a spin system can be expressed as

$$H_{\mathrm{hfi}} = A_x S_x I_x + A_y S_y I_y + A_z S_z I_z \quad (1)$$

where A refers to hyperfine coupling constant, S means spin angular momenta and I is nuclear spin. And in an axisymmetric system,

$$H_{\mathrm{hfi}} = A_\perp (S_x I_x + S_y I_y) + A_\parallel S_z I_z \quad (2)$$

herein, $a_x = a_y = a_\perp$, $a_z = a_\parallel$, $g_x = g_y = g_\perp$, $g_z = g_\parallel$. For $Y_2@C_{79}N$⊂MOF-177 complex, its axisymmetric hyperfine couplings at low temperature indicate that the $Y_2@C_{79}N$ molecules have directivity inside the matrix of MOF-177 crystal. However, the varied temperature ESR spectra performed on $Y_2@C_{79}N$ powders from 293 to 133 K (Figure 3c) exhibited unsplitting peak with a line width of *ca.* 18 G as the similar case in its solution state at 133 K due to the fast spin−lattice relaxation process.

Orientation of $Y_2@C_{79}N$ in $Y_2@C_{79}N$⊂MOF-177 Complex. This axisymmetric paramagnetic system of $Y_2@C_{79}N$⊂MOF-177 can be caused by the special structure of crystalline MOF-177 matrix, which has a trigonal space group of $P\bar{3}1c$.[8a] For MOF-177, its cage-shaped pore also has a quasi-planar moiety composed by triphenylbenzene unit. Therefore, it can be speculated that in $Y_2@C_{79}N$⊂MOF-177 complex, some site of $Y_2@C_{79}N$ would be close to the triphenylbenzene unit of MOF-177 through $\pi-\pi$ interactions. Especially under low temperature, the motion of $Y_2@C_{79}N$ molecule becomes slow in $Y_2@C_{79}N$⊂MOF-177 complex.

To further explicate the relative orientation of $Y_2@C_{79}N$ in $Y_2@C_{79}N$⊂MOF-177 complex, a model between $Y_2@C_{79}N$ and MOF-177 unit was constructed (Figure 4). DFT calculation results indicated that it is a favorable state that the N atom of $Y_2@C_{79}N$ situates near the paraphenylene unit of MOF-177 matrix, which is 2.08 kcal mol^{-1} more stable than

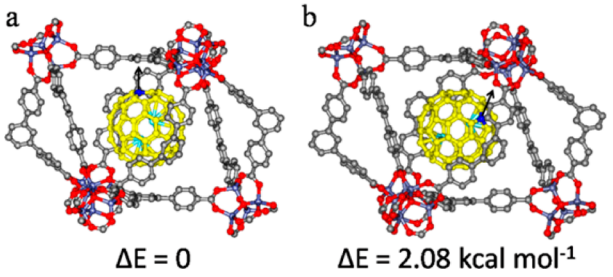

Figure 4. DFT-calculated geometries and relative energies (ΔE in kcal mol^{-1}) for a model of $Y_2@C_{79}N$⊂MOF-177. (a) The N atom (dark blue) on the carbon cage is pointed to the triphenylbenzene unit parallel to the *c* axis of MOF-177. (b) The N atom is pointed to one Zn_4O tetrahedron. Color code: light blue, Zn; red, O; gray, C_{MOF}; green, Y; dark blue, N; yellow, C_{cage}. H atoms and guest molecules are omitted for clarity.

that the N atom pointed to Zn_4O tetrahedron. On the other hand, the nearest distance between the N atom and the paraphenylene unit in Figure 4a is 3.58 Å, which is comparable with the distance of $\pi-\pi$ interaction in fullerene-containing host−guest complex[14] and much shorter than the distance (6.78 Å) between the N atom and the Zn_4O tetrahedron in Figure 4b.

It should be noted that the geometries of $Y_2@C_{79}N$ in MOF-177 pore are related to the different interactions between $Y_2@C_{79}N$ and triphenylbenzene unit. In several reported literatures, a strong interaction between a nitrogen-containing aromatic unit and a neutral π system has been determined.[15] For example; Tsuzuki and Sherrill reported that in benzene/pyridine complexes the orientation of N atom favors the structures in which the heteronitrogen atom is located toward the benzene molecule.[15a] Similarly, in $Y_2@C_{79}N$⊂MOF-177 complex, the substitution of N atom on fullerene cage also results in strong $\pi-\pi$ interaction between $Y_2@C_{79}N$ and benzene unit in MOF-177. In optimized structure of $Y_2@C_{79}N$⊂MOF-177 complex as shown in Figure 4a, the N-containing hexatomic ring is parallel to the central benzene unit of triphenylbenzene in MOF-177 through π-stacking interaction. This configuration is more stable than that in Figure 4b, in which the hexatomic carbon ring of $Y_2@C_{79}N$ is close to the central benzene unit of triphenylbenzene.

Therefore, it is rational that the $Y_2@C_{79}N$ is likely to situate along the *c* axis of MOF-177 crystal as in Figure 4a. In the presence of N and triphenylbenzene interactions, $Y_2@C_{79}N$ molecules tamely tend to align along the *c* axis ([001] crystal orientation) of MOF-177 crystal, as shown in Figure 1g. Consequently, at low temperature the axisymmetric hyperfine splittings can be observed.

Paramagnetic Property of $Y_2@C_{79}N$⊂MOF-177 Single Crystals with Different $Y_2@C_{79}N$ Loading Amount. The paramagnetic properties of $Y_2@C_{79}N$⊂MOF-177 single crystals with different loading amount of $Y_2@C_{79}N$ were also investigated, as shown in Figure 5. Briefly, three similar $Y_2@C_{79}N$⊂MOF-177 single crystal samples containing different weight content of $Y_2@C_{79}N$, i.e., 2%, 5% and 10%, were prepared. Their ESR spectra were collected at 130 K. The results revealed that $Y_2@C_{79}N$⊂MOF-177 single crystals exhibit nearly the same ESR hyperfine couplings, except for the enhanced signal intensity along with increased loading amount of $Y_2@C_{79}N$. Therefore, it can be noted that such axisymmetric ESR character for $Y_2@C_{79}N$⊂MOF-177 single

DOI: 10.1021/jacs.5b10796
J. Am. Chem. Soc. 2015, 137, 15055−15060

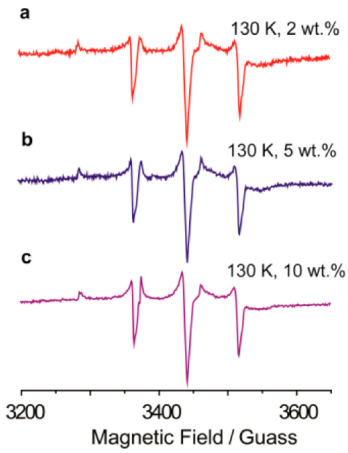

Figure 5. ESR spectra measured at 130 K for three $Y_2@C_{79}N$⊂MOF-177 single crystal samples containing different weight content of $Y_2@C_{79}N$. (a) 2%, (b) 5% and (c) 10%, respectively.

crystals is independent with the $Y_2@C_{79}N$ loading amount to a certain degree. This content-independent paramagnetic property can be attributed to a reason that the $Y_2@C_{79}N$ molecules are highly dispersed in the pores of MOF-177 under the loading amount ranging from 2% to 10%. Therefore, it is obvious that the pores in MOF-177 crystal play a significant role in accommodating and dispersing the $Y_2@C_{79}N$ molecules.

SQUID Measurement of $Y_2@C_{79}N$⊂MOF-177 Complex. Magnetic properties of this new complex were then studied by SQUID measurement as shown in Figure 6. The temperature-

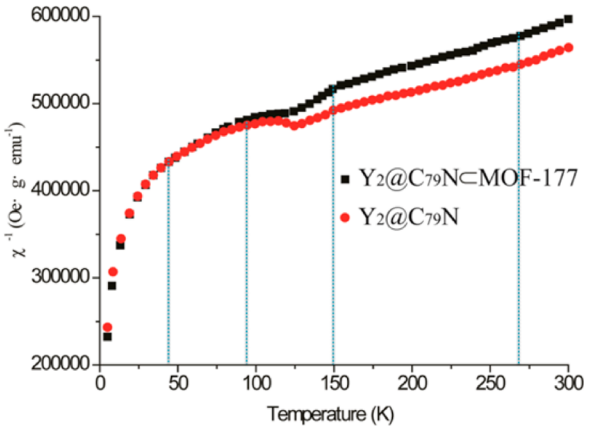

Figure 6. Temperature-dependent inverse magnetic susceptibility curves of $Y_2@C_{79}N$ (red circle) and $Y_2@C_{79}N$⊂MOF-177 (black square) measured at a field of 1000 Oe with temperature range of 5−300 K.

dependent inverse susceptibility of $Y_2@C_{79}N$⊂MOF-177 complex mainly featured a paramagnetic characteristic.[16−18] Fitting the susceptibility curve by the Curie−Weiss law provides C = 10.75 emu K mol^{-1} Oe^{1-}, Θ = −364.41 K (40−90 K); C = 23.04 emu K mol^{-1} Oe^{1-}, Θ = −898.57 K (150−260 K); and C = 18.57 emu K mol^{-1} Oe^{1-}, Θ = −671.59 K (260−300 K), respectively. Comparing the obtained magnetic parameters of $Y_2@C_{79}N$ powder and $Y_2@C_{79}N$⊂MOF-177 complex in Table S1, it can be derived that above 260 K their Curie constants are of almost the same value corresponding to the similar dynamical states of $Y_2@C_{79}N$ molecules in solid powders and inside the cavity of MOF-177, whereas below 260 K a slight decrease of Curie constant for $Y_2@C_{79}N$⊂MOF-177 was observed, which may be caused by the two possible orientations for $Y_2@C_{79}N$ in the cavity of MOF-177 as disclosed by above ESR results. In addition, an antiferromagnetic-like behavior occurred around 125 K for both $Y_2@C_{79}N$ powder and $Y_2@C_{79}N$⊂MOF-177, indicating a magnetic moment transition for $Y_2@C_{79}N$ molecules under such condition. Similar results were also found in solvent-free $Sc@C_{82}$ microcrystals[17] and $La@C_{82}(CS_2)_{1.5}$ crystals.[18]

CONCLUSION

We take advantage of MOFs to accommodate spin-active endohedral fullerene $Y_2@C_{79}N$. The ESR results revealed that the pores in MOF-177 crystal can highly disperse the $Y_2@C_{79}N$ molecules. In $Y_2@C_{79}N$⊂MOF-177 single crystal, the metallofullerene molecules are somewhat directional inside the pores of MOF crystal under low temperature and exhibit axisymmetric paramagnetic property. The $\pi-\pi$ interaction between N-containing hexatomic ring in $Y_2@C_{79}N$ and triphenylbenzene in MOF-177 helps to build such an axisymmetric paramagnetic system. This work provides an effective method to build a new solid spin system, which is similar to the paramagnetic diamond with nitrogen-vacancy centers. The NV-center diamond is known to be applicable in quantum computation and nanoscale nuclear magnetic resonance.[19] Compared to NV-center diamond, the $Y_2@C_{79}N$⊂MOF-177 solid spin system has controllable spin numbers and feasible fabrication process via a bottom-up approach. In addition, paramagnetic metallofullerene has been proved to be sensitive to the nitroxide radical with very weak magnetic field.[1h] Therefore, the $Y_2@C_{79}N$⊂MOF-177 solid spin system can be utilized in probing the motion of biomolecules, such as protein, labeled with nitroxide radical.

EXPERIMENTAL SECTION

Synthesis of MOF-177. MOF-177 was prepared by the solvothermal method as previously reported.[7e] Briefly, 80 mg of $Zn(NO_3)_2{\cdot}6H_2O$ and 20 mg of H_3BTB were dissolved in 1 mL of DEF, then the solution was sealed in a glass tube and heated at a rate of 2 °C/min to 100 °C and held for 23 h, and cooled at a rate of 0.2 °C/min to room temperature. The as-synthesized crystals were rinsed with DEF and toluene, respectively, each three times.

Characterizations of MOF-177. Single crystal X-ray diffraction (XRD), TGA, element analyses were carried out for structural characterization of MOF-177. For details, please see Figures S2 and S3 in the Supporting Information.

Synthesis of $Y_2@C_{79}N$⊂MOF-177. About 5 mg of MOF-177 crystals were immersed in a solution of 0.5 mg of $Y_2@C_{79}N$ in toluene for 7 days until the color of the crystals changed to orange. The doped crystals were washed with toluene (5 × 2 mL) and dried under N_2 flow.

Characterizations of $Y_2@C_{79}N$⊂MOF-177. TEM images and element mapping analysis were characterized by a JEOL 1011 instrument. Nitrogen adsorption/desorption isotherm was measured by a Quantachrome Autosorb AS-1 instrument at 77 K. PXRD and XPS were performed using the doped crystals at room temperature. XPS was performed on the Thermo Scientific ESCALab 250Xi using 200 W monochromated Al Kα radiation. The 500 μm X-ray spot was used for XPS analysis. The base pressure in the analysis chamber was about 3 × 10^{-10} mbar. Typically the hydrocarbon C 1s line at 284.8 eV from adventitious carbon is used for energy referencing. Weight ratio was calculated by ICP results: ca. 3.29 mg of $Y_2@C_{79}N$⊂MOF-177 crystals were dissolved in 2 mL of HNO_3, sonicated for 30 min and then transferred to a mixture of H_2SO_4/H_2O_2 (v/v = 4/1), sonicated for another 30 min. This acid solution was diluted 1000 times and detected the Y^{3+} and Zn^{2+} on SHIMADZU ICPE-90000 instrument.

DOI: 10.1021/jacs.5b10796
J. Am. Chem. Soc. 2015, 137, 15055−15060

ESR Measurements of $Y_2@C_{79}N$⊂MOF-177. The varied temperature ESR spectra for $Y_2@C_{79}N$⊂MOF-177 were recorded on Bruker E500 instrument with continuous-wave X band. And the spectra were simulated with Easyspin package[20] (http://www.easyspin.org) encoded in MATLAB platform.

SQUID Measurements of $Y_2@C_{79}N$⊂MOF-177. The susceptibility experiments were performed on a Quantum Design MPMS XL-7 system at temperature from 5 to 300 K in magnetic field of 0.1 T. The sample was sealed in a capsule with negligible magnetism.

■ ASSOCIATED CONTENT

Supporting Information

The Supporting Information is available free of charge on the ACS Publications website at DOI: 10.1021/jacs.5b10796.

Experimental details, TGA, PXRD, XPS, ESR profiles and calculation results. (PDF)
Crystallographic data. (CIF)

■ AUTHOR INFORMATION

Corresponding Authors

*wangtais@iccas.ac.cn
*crwang@iccas.ac.cn

Notes

The authors declare no competing financial interest.

■ ACKNOWLEDGMENTS

This work was supported by the National Key Basic Research Program (2012CB932901), National Natural Science Foundation of China (21203205, 61227902, 51472248), NSAF (11179006), and the Key Research Program of the Chinese Academy of Sciences (KGZD-EW-T02). T. Wang particularly thanks the Youth Innovation Promotion Association of CAS.

■ REFERENCES

(1) (a) Bogani, L.; Wernsdorfer, W. *Nat. Mater.* **2008**, *7*, 179. (b) Rocha, A. R.; Garcia-Suarez, V. M.; Bailey, S. W.; Lambert, C. J.; Ferrer, J.; Sanvito, S. *Nat. Mater.* **2005**, *4*, 335. (c) Wolf, S.; Awschalom, D.; Buhrman, R.; Daughton, J.; Von Molnar, S.; Roukes, M.; Chtchelkanova, A. Y.; Treger, D. *Science* **2001**, *294*, 1488. (d) Rao, A.; Chow, P. C.; Gélinas, S.; Schlenker, C. W.; Li, C.-Z.; Yip, H.-L.; Jen, A. K.-Y.; Ginger, D. S.; Friend, R. H. *Nature* **2013**, *500*, 435. (e) Du, J.; Rong, X.; Zhao, N.; Wang, Y.; Yang, J.; Liu, R. *Nature* **2009**, *461*, 1265. (f) Morton, J. J.; Tyryshkin, A. M.; Brown, R. M.; Shankar, S.; Lovett, B. W.; Ardavan, A.; Schenkel, T.; Haller, E. E.; Ager, J. W.; Lyon, S. *Nature* **2008**, *455*, 1085. (g) Kato, Y.; Myers, R.; Driscoll, D.; Gossard, A.; Levy, J.; Awschalom, D. *Science* **2003**, *299*, 1201. (h) Wu, B.; Wang, T.; Feng, Y.; Zhang, Z.; Jiang, L.; Wang, C. *Nat. Commun.* **2015**, *6*, 6468.

(2) (a) Chappert, C.; Fert, A.; Van Dau, F. N. *Nat. Mater.* **2007**, *6*, 813. (b) Ladd, T. D.; Jelezko, F.; Laflamme, R.; Nakamura, Y.; Monroe, C.; O'Brien, J. L. *Nature* **2010**, *464*, 45. (c) Du, J.; Li, H.; Xu, X.; Shi, M.; Wu, J.; Zhou, X.; Han, R. *Phys. Rev. Lett.* **2002**, *88*, 137902. (d) Du, J.; Durt, T.; Zou, P.; Li, H.; Kwek, L. C.; Lai, C.; Oh, C.; Ekert, A. *Phys. Rev. Lett.* **2005**, *94*, 040505. (e) Friesen, M.; Tahan, C.; Joynt, R.; Eriksson, M. *Phys. Rev. Lett.* **2004**, *92*, 037901. (f) Hueso, L. E.; Pruneda, J. M.; Ferrari, V.; Burnell, G.; Valdés-Herrera, J. P.; Simons, B. D.; Littlewood, P. B.; Artacho, E.; Fert, A.; Mathur, N. D. *Nature* **2007**, *445*, 410. (g) Steger, M.; Saeedi, K.; Thewalt, M.; Morton, J.; Riemann, H.; Abrosimov, N.; Becker, P.; Pohl, H.-J. *Science* **2012**, *336*, 1280. (h) Maurer, P. C.; Kucsko, G.; Latta, C.; Jiang, L.; Yao, N. Y.; Bennett, S. D.; Pastawski, F.; Hunger, D.; Chisholm, N.; Markham, M. *Science* **2012**, *336*, 1283. (i) Boehme, C.; McCamey, D. R. *Science* **2012**, *336*, 1239.

(3) (a) Popov, A. A.; Yang, S.; Dunsch, L. *Chem. Rev.* **2013**, *113*, 5989. (b) Yamada, M.; Akasaka, T.; Nagase, S. *Acc. Chem. Res.* **2009**, *43*, 92. (c) Turro, N. J.; Chen, J. Y.-C.; Sartori, E.; Ruzzi, M.; Marti, A.; Lawler, R.; Jockusch, S.; López-Gejo, J.; Komatsu, K.; Murata, Y. *Acc. Chem. Res.* **2009**, *43*, 335. (d) Dunk, P. W.; Adjizian, J.-J.; Kaiser, N. K.; Quinn, J. P.; Blakney, G. T.; Ewels, C. P.; Marshall, A. G.; Kroto, H. W. *Proc. Natl. Acad. Sci. U. S. A.* **2013**, *110*, 18081.

(4) (a) Harneit, W.; Meyer, C.; Weidinger, A.; Suter, D.; Twamley, J. *Phys. Status Solidi B* **2002**, *233*, 453. (b) Grose, J. E.; Tam, E. S.; Timm, C.; Scheloske, M.; Ulgut, B.; Parks, J. J.; Abruna, H. D.; Harneit, W.; Ralph, D. C. *Nat. Mater.* **2008**, *7*, 884. (c) Harneit, W. *Phys. Rev. A: At., Mol., Opt. Phys.* **2002**, *65*, 032322. (d) Meyer, C.; Harneit, W.; Weidinger, A.; Lips, K. *Phys. Status Solidi B* **2002**, *233*, 462.

(5) (a) Corzilius, B.; Jakes, P.; Weiden, N.; Agarwal, S.; Dinse, K.-P. *Mol. Phys.* **2007**, *105*, 2161. (b) Liu, G.; Gimenez-Lopez, M. d. C.; Jevric, M.; Khlobystov, A. N.; Briggs, G. A. D.; Porfyrakis, K. *J. Phys. Chem. B* **2013**, *117*, 5925.

(6) (a) Guan, L.; Suenaga, K.; Shi, Z.; Gu, Z.; Iijima, S. *Phys. Rev. Lett.* **2005**, *94*, 045502. (b) Ge, L.; Jefferson, J. H.; Montanari, B.; Harrison, N. M.; Pettifor, D. G.; Briggs, G. A. D. *ACS Nano* **2009**, *3*, 1069. (c) Hornbaker, D.; Kahng, S.-J.; Misra, S.; Smith, B.; Johnson, A.; Mele, E.; Luzzi, D.; Yazdani, A. *Science* **2002**, *295*, 828. (d) Hirahara, K.; Suenaga, K.; Bandow, S.; Kato, H.; Okazaki, T.; Shinohara, H.; Iijima, S. *Phys. Rev. Lett.* **2000**, *85*, 5384. (e) Iwamoto, T.; Watanabe, Y.; Sadahiro, T.; Haino, T.; Yamago, S. *Angew. Chem.* **2011**, *123*, 8492.

(7) (a) Farha, O. K.; Hupp, J. T. *Acc. Chem. Res.* **2010**, *43*, 1166. (b) Chen, B.; Xiang, S.; Qian, G. *Acc. Chem. Res.* **2010**, *43*, 1115. (c) Wang, Z.; Cohen, S. M. *Chem. Soc. Rev.* **2009**, *38*, 1315. (d) Stock, N.; Biswas, S. *Chem. Rev.* **2011**, *112*, 933. (e) Chae, H. K.; Siberio-Pérez, D. Y.; Kim, J.; Go, Y.; Eddaoudi, M.; Matzger, A. J.; O'Keeffe, M.; Yaghi, O. M. *Nature* **2004**, *427*, 523.

(8) (a) Inokuma, Y.; Arai, T.; Fujita, M. *Nat. Chem.* **2010**, *2*, 780. (b) Rao, D.; Lu, R.; Xiao, C.; Kan, E.; Deng, K. *Chem. Commun.* **2011**, *47*, 7698. (c) Peng, P.; Li, F. F.; Neti, V. S. P. K.; Metta-Magana, A. J.; Echegoyen, L. *Angew. Chem., Int. Ed.* **2014**, *53*, 160. (d) García-Simón, C.; Garcia-Borràs, M.; Gómez, L.; Parella, T.; Osuna, S.; Juanhuix, J.; Imaz, I.; Maspoch, D.; Costas, M.; Ribas, X. *Nat. Commun.* **2014**, *5*, 5557. (e) Hitosugi, S.; Ohkubo, K.; Iizuka, R.; Kawashima, Y.; Nakamura, K.; Sato, S.; Kono, H.; Fukuzumi, S.; Isobe, H. *Org. Lett.* **2014**, *16*, 3352. (f) Nakanishi, Y.; Omachi, H.; Matsuura, S.; Miyata, Y.; Kitaura, R.; Segawa, Y.; Itami, K.; Shinohara, H. *Angew. Chem., Int. Ed.* **2014**, *53*, 3102. (g) Hajjaj, F.; Tashiro, K.; Nikawa, H.; Mizorogi, N.; Akasaka, T.; Nagase, S.; Furukawa, K.; Kato, T.; Aida, T. *J. Am. Chem. Soc.* **2011**, *133*, 9290. (h) García-Simón, C.; Gramage-Doria, R.; Raoufmoghaddam, S.; Parella, T.; Costas, M.; Ribas, X.; Reek, J. N. *J. Am. Chem. Soc.* **2015**, *137*, 2680.

(9) (a) Zuo, T.; Xu, L.; Beavers, C. M.; Olmstead, M. M.; Fu, W.; Crawford, T. D.; Balch, A. L.; Dorn, H. C. *J. Am. Chem. Soc.* **2008**, *130*, 12992. (b) Ma, Y.; Wang, T.; Wu, J.; Feng, Y.; Jiang, L.; Shu, C.; Wang, C. *Chem. Commun.* **2012**, *48*, 11570.

(10) (a) Huang, P.; Kong, X.; Zhao, N.; Shi, F.; Wang, P.; Rong, X.; Liu, R.-B.; Du, J. *Nat. Commun.* **2011**, *2*, 570. (b) Maletinsky, P.; Hong, S.; Grinolds, M. S.; Hausmann, B.; Lukin, M. D.; Walsworth, R. L.; Loncar, M.; Yacoby, A. *Nat. Nanotechnol.* **2012**, *7*, 320.

(11) (a) Pyser, J. B.; Aulakh, D.; Zhang, X.; Yakovenko, A. A.; Dunbar, K. R.; Wriedt, M. *J. Am. Chem. Soc.* **2015**, *137*, 9254. (b) Minar, N. K.; Hou, K.; Westermeier, C.; Döblinger, M.; Schuster, J.; Hanusch, F. C.; Nickel, B.; Ozin, G. A.; Bein, T. *Angew. Chem.* **2015**, *127*, 7687.

(12) Kato, T.; Bandou, S.; Inakuma, M.; Shinohara, H. *J. Phys. Chem.* **1995**, *99*, 856.

(13) Kincer, M. R.; Choudhury, R.; Srinivasarao, M.; Beckham, H. W.; Briggs, G. A. D.; Porfyrakis, K.; Bucknall, D. G. *Polymer* **2015**, *56*, 516.

(14) Iwamoto, T.; Slanina, Z.; Mizorogi, N.; Guo, J.; Akasaka, T.; Nagase, S.; Takaya, H.; Yasuda, N.; Kato, T.; Yamago, S. *Chem. - Eur. J.* **2014**, *20*, 14403.

(15) (a) Tsuzuki, S.; Mikami, M.; Yamada, S. *J. Am. Chem. Soc.* **2007**, *129*, 8656. (b) Hohenstein, E. G.; Sherrill, C. D. *J. Phys. Chem. A* **2009**,

DOI: 10.1021/jacs.5b10796
J. Am. Chem. Soc. 2015, 137, 15055−15060

113, 878. (c) Li, P.; Zhao, C.; Smith, M. D.; Shimizu, K. D. *J. Org. Chem.* **2013**, *78*, 5303.
(16) Funasaka, H.; Sugiyama, K.; Yamamoto, K.; Takahashi, T. *J. Phys. Chem.* **1995**, *99*, 1826.
(17) Ito, Y.; Fujita, W.; Okazaki, T.; Sugai, T.; Awaga, K.; Nishibori, E.; Takata, M.; Sakata, M.; Shinohara, H. *ChemPhysChem* **2007**, *8*, 1019.
(18) Nuttall, C.; Inada, Y.; Nagai, K.; Iwasa, Y. *Phys. Rev. B: Condens. Matter Mater. Phys.* **2000**, *62*, 8592.
(19) (a) Mamin, H.; Kim, M.; Sherwood, M.; Rettner, C.; Ohno, K.; Awschalom, D.; Rugar, D. *Science* **2013**, *339*, 557. (b) Zu, C.; Wang, W.-B.; He, L.; Zhang, W.-G.; Dai, C.-Y.; Wang, F.; Duan, L.-M. *Nature* **2014**, *514*, 72. (c) Staudacher, T.; Shi, F.; Pezzagna, S.; Meijer, J.; Du, J.; Meriles, C.; Reinhard, F.; Wrachtrup, J. *Science* **2013**, *339*, 561. (d) Shi, F.; Zhang, Q.; Wang, P.; Sun, H.; Wang, J.; Rong, X.; Chen, M.; Ju, C.; Reinhard, F.; Chen, H.; Wrachtrup, J.; Wang, J.; Du, J. *Science* **2015**, *347*, 1135.
(20) (a) Stoll, S.; Schweiger, A. *J. Magn. Reson.* **2006**, *178*, 42−55. (b) Stoll, S.; Schweiger, A. *Chem. Phys. Lett.* **2003**, *380*, 464−470.

DOI: 10.1021/jacs.5b10796
J. Am. Chem. Soc. 2015, 137, 15055−15060